Fungal Biology 129 (2025) 101549

Contents lists available at ScienceDirect

Fungal Biology

journal homepage: www.elsevier.com/locate/funbio

Revealing robust antioxidant defences of a mycoparasitic *Trichoderma* species

Siebe Pierson [a], Mark Fricker [b], Alexander Lichius [a,c], Adolf Michael Sandbichler [d], Susanne Zeilinger [a,*]

[a] Department of Microbiology, University of Innsbruck, Innsbruck, Austria
[b] Department of Biology, University of Oxford, Oxford, United Kingdom
[c] Inncellys GmbH, Mils, Austria
[d] Department of Zoology, University of Innsbruck, Innsbruck, Austria

ARTICLE INFO

Handling Editor: Dr D.E.N. Rangel

Keywords:
Trichoderma asperellum
Grx1-roGFP2
Glutathione
Confocal redox imaging
Reactive oxygen species (ROS)

ABSTRACT

The fungal genus *Trichoderma* contains a vast array of species well known for their high opportunistic potential and adaptability to various ecological niches. The ability of many *Trichoderma* species to both colonize the rhizosphere and parasitize plant pathogenic fungi has led to their use in biological pathogen control for several decades. Reactive oxygen species (ROS) are linked to both the antagonism imposed by the mycoparasite *Trichoderma* and the elicited defence reaction by its fungal hosts during the mycoparasitic interaction. *Trichoderma* spp. likely tolerate higher levels of ROS compared with some of their host species, thereby giving them an advantage during the mycoparasitic interaction.

In the present study, we investigated glutathione redox dynamics using the fluorescent reporter Grx1-roGFP2 stably expressed in *Trichoderma asperellum* following electrotransformation. Grx1-roGFP2 undergoes reversible changes in its excitation spectrum in response to variations in the cellular glutathione redox potential, providing a real-time indication of intracellular oxidative load. Considering the putative importance of ROS in mycoparasitic interactions, we performed live-cell imaging of the *T. asperellum* reporter strain interacting with the cereal pathogen *Fusarium graminearum*. Surprisingly, the glutathione redox potential did not change during this mycoparasitic interaction. We found no evidence that host-induced tip growth arrest within *T. asperellum* hyphae is induced by intracellular ROS accumulation. Furthermore, we show that the *F. graminearum* mycotoxins deoxynivalenol and zearalenone do not induce detectable changes in glutathione redox potential, even at very high concentrations. We infer that *T. asperellum* has a robust anti-oxidant defence system, supported by the observation that high concentrations of H_2O_2 are required to fully oxidize the reporter during *in vivo* calibration. We cannot rule out a role for ROS as a signal during mycoparasitic interactions, but, if present, this does not appear to be mediated by glutathione redox potential.

1. Introduction

Trichoderma species are cosmopolitan soilborne ascomycetes and have emerged as pivotal players in sustainable agriculture. Their ability to both colonize the rhizosphere and parasitize plant pathogenic fungi has led to their use in biological pest control for several decades (Guzmán-Guzmán et al., 2023; Tyśkiewicz et al., 2022; Woo et al., 2023). Upon interaction with a plant, certain species of the *Trichoderma* genus induce a wide range of cellular responses, including disease suppression, enhanced photosynthesis, improved nutrient uptake, drought tolerance, and phytohormone secretion (Contreras-Cornejo et al., 2024; Tyśkiewicz et al., 2022). Additionally, through a process termed mycoparasitism, *Trichoderma* spp. antagonize plant pathogenic fungi and thereby further improve plant survival (Druzhinina et al., 2011; Guzmán-Guzmán et al., 2023). *Trichoderma asperellum* is among the *Trichoderma* spp. with the most effective biocontrol properties and is

This article is part of a special issue entitled: ISFUS-V published in Fungal Biology.

* Corresponding author.
E-mail addresses: siebe.pierson@uibk.ac.at (S. Pierson), mark.fricker@biology.ox.ac.uk (M. Fricker), innovate@inncellys.com (A. Lichius), adolf.sandbichler@uibk.ac.at (A.M. Sandbichler), susanne.zeilinger@uibk.ac.at (S. Zeilinger).

https://doi.org/10.1016/j.funbio.2025.101549
Received 8 November 2024; Received in revised form 7 February 2025; Accepted 10 February 2025
Available online 15 February 2025

therefore widely used in biocontrol applications (Tyśkiewicz et al., 2022).

Trichoderma spp. engage in mycoparasitic interactions with a host fungus to exploit it as nutrient source (Barnett, 1963). Throughout this interaction, both *Trichoderma* and the host fungus experience extensive stress as a result of the opposing partner's defence responses. Upon microscopic analysis of these interactions, hyphal tip growth arrest of hyphae at the interaction zone is one of the main stress phenotypes that can be observed (Druzhinina et al., 2011; Karlsson et al., 2017; Moreno-Ruiz et al., 2021). Druzhinina et al. (2011) suggest that the stress responses in *Trichoderma* spp. are elicited by both antifungal metabolites and reactive oxygen species (ROS) produced by the host fungus. Thus, it is possible that hyphal tip growth arrest during the mycoparasitic interaction might result from ROS accumulation within *T. asperellum* hyphae. This is similar in mammalian cells, where the accumulation of intracellular ROS has been associated with growth arrest (Boonstra and Post, 2004; Kuczler et al., 2021).

Hyphal tip growth can be monitored with the CRIB reporter system. Previously optimised for *Trichoderma atroviride* (Moreno-Ruiz et al., 2021), the CRIB reporter system enables the distinction between actively growing hyphae and those with disrupted tip growth. The CRIB reporter consists of a Cdc42/Rac1-interactive binding (CRIB) motif linked to a fluorescent protein. This fusion protein specifically associates with active Rho-type GTPases, such as Cdc42 and Rac1, which are key regulators of hyphal tip polarity (Lichius et al., 2014; Riquelme and Martínez-Núñez, 2016). Since these GTPases are essential for active hyphal growth, the fluorescence accumulation at the tip apex indicates activation of the GTPases and thus active hyphal extension (Moreno-Ruiz et al., 2021).

Supraphysiological ROS concentrations within the cell pose a threat by oxidizing essential lipids, proteins and nucleic acids (Aguirre et al., 2006; Di Meo et al., 2016; Gessler et al., 2007; Tudzynski et al., 2012; Yaakoub et al., 2022). It is well established that part of the plant defence mechanism during the interaction with fungal phytopathogens is the overproduction of ROS at the infection site. This oxidative burst results in localized cell death of invading fungal cells at the infection site (Singh et al., 2021). Conversely, several studies indicate that necrotrophic phytopathogens such as *Botrytis cinerea* efficiently produce ROS as part of their infection strategy to kill the plant without themselves experiencing oxidative stress (Heller and Tudzynski, 2011; Mentges and Bormann, 2015; Warris and Ballou, 2019). Other plant pathogens, such as *Fusarium* spp. have a particularly strong potential to induce ROS production through the biosynthesis of potent mycotoxins such as zearalenone (ZEN) and deoxynivalenol (DON). Both mycotoxins have been linked to oxidative stress induction in plants and mammalian cells (De Nijs et al., 1997; Favero et al., 2018; Feng et al., 2022; Filek et al., 2019; Mishra et al., 2014; Waśkiewicz et al., 2014; Yoon et al., 2019), with oxidative stress defined when the intracellular ROS concentration exceeds the antioxidant capacity of the cell (Sies, 1991).

Here, we focus on the interaction between *T. asperellum* and *F. graminearum*, a widespread pathogen of small grain cereals causing Fusarium head blight (Goswami and Kistler, 2004; Parry et al., 1995). Analogous to these phytopathogens, *Trichoderma* spp. also have the ability to produce ROS, notably through plasma membrane NADPH oxidases (Nox). Such ROS production has been linked to antagonism against phytopathogens such as *Pythium ultimum* (Hernández-Oñate et al., 2012; Montero-Barrientos et al., 2011). Furthermore, Morán-Diez et al. (2021) even suggest that *Trichoderma* spp. have the ability to tolerate higher levels of ROS compared with some of their host species, thus giving them an advantage during the mycoparasitic interaction.

Fungi have evolved various enzymatic and non-enzymatic systems to inhibit ROS from oxidizing essential cell structures and causing irreversible cell damage. An oxidative load is mitigated by an array of sophisticated antioxidant defence systems, thus resulting in an intricate balance of intracellular ROS (Aguirre et al., 2006; Belozerskaya and Gessler, 2007; Gessler et al., 2007; Yaakoub et al., 2022). Given the hostile environment *Trichoderma* spp. face upon interaction with a host fungus, an effective antioxidant system is likely essential for the ability of *Trichoderma* spp. to successfully exploit their hosts (Morán-Diez et al., 2021). Although many studies report the ability of *Trichoderma* spp. to stimulate the antioxidant defence system of plants (Ahmad et al., 2015; S. Chen et al., 2020; S.-C. Chen et al., 2019; Mastouri et al., 2012), our understanding of the antioxidant defences within the fungus itself remains incomplete, particularly during mycoparasitic interactions. For example, it is unclear whether or how *Trichoderma* spp. tolerate higher ROS levels compared to some of their host species. This highlights the need for novel strategies to study these topics.

T. asperellum produces superoxide dismutase and, together with catalase, these enzymes remove potentially harmful ROS (Gao et al., 2018). Other enzymes involved in antioxidant activity are glutathione S-transferase, glutathione peroxidase and peroxidase (Ernesto Juniors et al., 2020). Nevertheless, the primary antioxidant system in eukaryotes is centred around glutathione (Aquilano et al., 2014; Meyer, 2008) which neutralises oxidative loads through the reversible conversion of its reduced form (GSH) to its oxidized form (GSSG), thereby reducing intracellular ROS (Belozerskaya and Gessler, 2007; Meyer, 2008). The genetically encoded fluorescence reporter Grx1-roGFP2 allows us to monitor the reversible conversion between GSH and GSSG in real-time and is therefore ideal for observing the impact of any oxidative load a cell is dealing with at a given timepoint. While initially optimised to target mitochondria in HeLa cells (Hanson et al., 2004), this fluorescent reporter has subsequently been used to study redox dynamics in the plant *Arabidopsis thaliana* and the fungal phytopathogens *B. cinerea* and *Magnaporthe oryzae* (Heller et al., 2012; Meyer et al., 2007; Samalova et al., 2014).

Grx1-roGFP2 combines the specificity of a glutaredoxin 1 (Grx1) protein with the redox-sensitive green fluorescent protein (roGFP2). roGFP2 is a variant of the green fluorescent protein (GFP) that undergoes a reversible conformational change in response to oxidation or reduction of its two cysteine residues. This conformational change, i.e. the presence (fully oxidized state) or absence (fully reduced state) of a disulfide bridge, alters the excitation spectrum of roGFP2. Oxidation of the cysteine residues results in increased excitation at 405 nm while cysteine reduction increases the 488 nm excitation peak. Importantly, the rate and extent of this shift in excitation wavelength are directly proportional to the redox potential of the environment surrounding the cysteine residues (Hanson et al., 2004). The sensitivity of the reporter system is determined by its midpoint redox potential. Given that the midpoint redox potential of roGFP2 (−280 mV) is lower than that of glutathione at physiological concentrations (ranging from −151 mV at 1 mM to −181 mV at 10 mM), even a slight increase in glutathione oxidation within the organism leads to substantial sensor oxidation (Dooley et al., 2004; Chuffart and Yvert, 2014; Gutscher et al., 2008; Schwarzländer et al., 2016). The fusion of roGFP2 with Grx1 enhances the specificity, response kinetics and sensitivity of the reporter. Glutaredoxins are thiol-disulfide oxidoreductases that play a central role in maintaining cellular redox homeostasis by catalysing the reduction of disulfide bonds in target proteins. Grx1 possesses a high affinity for glutathione (Ukuwela et al., 2018). Coupling Grx1 directly to the roGFP2 reporter ensures rapid responses to fluctuations in the GSH/GSSG ratio, providing a direct readout of cellular glutathione redox potential (Gutscher et al., 2008).

In this study, changes in the glutathione redox potential within *T. asperellum* hyphae in the absence and presence of the phytopathogenic fungus *F. graminearum* were investigated. First, we determined whether Grx1-roGFP2 can be functionally expressed in *T. asperellum* and reliably reports the glutathione redox potential during imposed oxidation or reduction. Second, we examined whether Grx1-roGFP2 reports a change in the glutathione redox potential during mycoparasitic interaction with *F. graminearum*. Third, we investigated whether hyphal tip growth arrest of *T. asperellum* during the mycoparasitic interaction is correlated with excess ROS accumulation within *T. asperellum* hyphae.

Finally, we investigated whether the *Fusarium* mycotoxins DON and ZEN induce oxidative stress in *T. asperellum*. By integrating both the Grx1-roGFP2 and CRIB reporter systems into the genome of *T. asperellum*, we aimed to develop a system to correlate fluctuations in the glutathione redox potential with the growth behaviour of individual *T. asperellum* hyphae. Overall, we seek to better understand the role of ROS in mycoparasitism and how *T. asperellum* mitigates and is affected by oxidative loads encountered in its vicinity and specifically upon contact with potential host fungi.

2. Materials & methods

2.1. Strains & culture conditions

Trichoderma asperellum CBS 433.97 was used as wild type (WT) for transformation with Grx1-roGFP2, to give transgenic strain *TarG* (***Tri**choderma **a**sperellum* **roG**FP2). For dual confrontation assays, *F. graminearum* strain 8/1 (Jansen et al., 2005) and *B. cinerea* strain B05.10 were used as host fungi. For each live-cell imaging session, conidia of *TarG* and *F. graminearum* were freshly generated. Conidia of *TarG* were generated through cultivation on Potato Dextrose Agar (PDA, BD Difco, Franklin Lakes, NJ, USA) at 25 °C under a 12h/12h light/dark cycle for 4 days. For *F. graminearum*, mycelial plug inocula were suspended in 50 mL mung bean broth and incubated at room temperature in a shaker at 150 rpm and a natural light/dark cycle. Mung bean broth was generated by boiling 40 g of mung beans in 1 L of water and filtering through three layers of Miracloth (Merck KGaA, Darmstadt, Germany). After 5–10 days of incubation, *F. graminearum* macroconidia were filtered out using sterile triple layered Miracloth (Merck KGaA, Darmstadt, Germany). Conidia of *B. cinerea* were generated through cultivation on PDA for 10 days at room temperature and a natural light/dark cycle (Meng et al., 2020). For live-cell imaging, conidia were cultivated on Modified M9 medium (MM9) with 1 % phytagel (Merck KGaA, Darmstadt, Germany) at 25 °C in darkness (Moreno-Ruiz et al., 2020).

2.2. Generation of T. asperellum Grx1-roGFP2 transformants

The fluorescent reporter Grx1-roGFP2 was transformed into WT *T. asperellum* through electrotransformation aiming for ectopic integration into the fungal genome. Plasmids with the reporter cassette for high-level cytoplasmic expression of Grx1-roGFP2 were generated as follows. Five fragments, each amplified through PCR using Q5 high-fidelity DNA polymerase (New England Biolabs, Ipswich, MA, USA) according to the manufacturer's instructions, were assembled. The backbone, a hygromycin B resistance-mediating cassette (*hph* cassette) and the CRIB motif from the p21-activated protein kinases (PAK)-like-kinase CLA-4 of *T. asperellum* (*crib(cla4)*) were amplified from plasmid pLS3-CRIBc-mBasicGFP (Moreno-Ruiz et al., 2021). The TagRFP-T fluorophore was amplified from plasmid pAL12-Lifeact (Lichius and Read, 2009). Finally, Grx1-roGFP2 was amplified from plasmid pBinCM-Grx1-roGFP2 (Gutscher et al., 2008), kindly provided by Markus Schwarzländer. The primers used are given in the supporting data (Table S1). Fragments were assembled with the NEBuilder® HiFi DNA Assembly Master Mix (New England Biolabs, Ipswich, MA, USA), resulting in plasmid pSP-CRIBc-TagRFP-T-Grx1-roGFP2 (P*pki*::*crib (cla4)-TagRFP-T,* P*tef1a*::*Grx1-roGFP2*) with the *hph* cassette positioned in between the CRIB reporter and Grx1-roGFP2. A detailed summary and illustration of the vector assembly is given in Table S2 and Fig. S1. The plasmid was propagated through *Escherichia coli* Stellar cells (Takara, Saint-Germain-en-Laye, FR) and selected plasmid clones were verified by colony-PCR using DreamTaq DNA polymerase (Thermo Fisher Scientific Inc., Bremen, Germany). Plasmids were extracted from *E. coli* using the Monarch Plasmid Miniprep kit (New England Biolabs, Ipswich, MA, USA). The fragment for fungal transformation was amplified from the plasmid through PCR using primers P1_F and P1_R (Table S1) and Q5 high-fidelity DNA polymerase (New England Biolabs, Ipswich, MA, USA) followed by purification using the Monarch PCR & DNA Cleanup kit (New England Biolabs, Ipswich, MA, USA).

For electroporation, freshly harvested *T. asperellum* conidia were allowed to swell for 6.5 h in yeast extract-peptone-dextrose (YPD) medium followed by a washing step and osmotic stabilisation with 1.1 M sorbitol solution. Re-useable cuvettes with a 0.2 cm gap width were loaded with 5 μg DNA fragment and 3×10^8 conidia suspended in 75 μL 1.1 M sorbitol solution. An electric shock of 1.8 kV (9 kV/cm field strength) was applied with a circuit resistance of 800 Ω and a capacitance of 25 μF using the BTX™ Gemini X2 Electroporation System (BTX, Harvard Bioscience inc., Holliston, MA, USA). After overnight recovery in YPDS (YPD medium containing 1 M sorbitol) the cells were plated on PDA medium amended with 1 M sorbitol and 500 μg/mL hygromycin B (Calbiochem, CA, USA) as selection agent.

Emerging transformants were analysed for fluorescent protein expression through live-cell imaging microscopy. A selection of transformants that showed strong fluorescence was purified to mitotic stability through three rounds of single spore isolation on PDA containing 500 μg/mL hygromycin B (Calbiochem, CA, USA). The purified transformants were subjected to a range of growth assays and their growth rate and phenotype (pigmentation, sporulation, mycelial density) were compared with WT *T. asperellum*. To this end, the following assays were performed: growth assays on PDA and minimal MM9 medium; stress assays on PDA in the presence of 1.2 M sorbitol (osmotic stress), 1 M NaCl (salt stress), 20 mM H_2O_2 (oxidative stress) or 200 μM Congo Red (cell wall stress); dual interaction assays on PDA using *B. cinerea* or *F. graminearum* as fungal hosts. Two transformant strains generated the highest fluorescence intensity and otherwise displayed an unaltered WT phenotype, one transformant was selected for subsequent experiments and hereafter referred to as *TarG* (Fig. 1). The subcellular localization of Grx1-roGFP2 and response to H_2O_2 and DTT exposure was highly similar in both transformants (Supplementary Fig. S2). The sequence encoding Grx1-roGFP2, within the genome, was verified through Sanger Sequencing (Microsynth AG, Balgach, CH) using primers Sanger_F and Sanger_R (Table S1).

2.3. Confocal imaging

Time series and images were acquired with a Leica SP5-II confocal laser scanning microscope (CLSM), using the LAS AF software (version 2.7.3, Leica Microsystems, Germany). The Leica SP5-II CLSM was equipped with a hybrid detector (HyD), a photomultiplier tube detector (PMT) and a 63 × (1.3 NA) glycerol-immersion objective lens. For ratio-imaging, the roGFP2 fluorophore was excited with a 405 nm and a 488 nm laser and the emission was detected at 500–550 nm with the HyD for both lasers. Additionally, at 405 nm excitation, a second detector was set to 435–485 nm to capture potential autofluorescence and allow its removal if necessary. Since no autofluorescence was observed, this channel was omitted from the results. Time series were collected at 30 s intervals for 14–30 min, with the focal plane set in the middle of the hypha of interest. The pinhole was set at 200 μm, resulting in an estimated optical section thickness of 1.5 μm, well within the width of *T. asperellum* hyphae (3–8 μm).

2.4. Live-cell imaging of dual confrontation and mycotoxin exposure

Axenic *TarG* cultures or dual confrontation cultures (*TarG* versus *F. graminearum*) were grown in inncelly® experimentation chambers ib02 (inncellys GmbH, Mils, AT). inncelly® chambers allow contamination-free yet aerated incubation as well as injury-free sample preparation of intact microcolonies for live-cell imaging analysis (Fig. 2). The exclusion of injury-induced stress artefacts was vital for the investigation of cellular oxidative stress responses in this context. inncelly® chambers contain a 75 × 50 mm glass cover slip on which 20 mL MM9 medium was poured. Fungal conidia were inoculated by pipetting a 5 μL drop of conidial suspension (1000 conidia/μL of *TarG* or

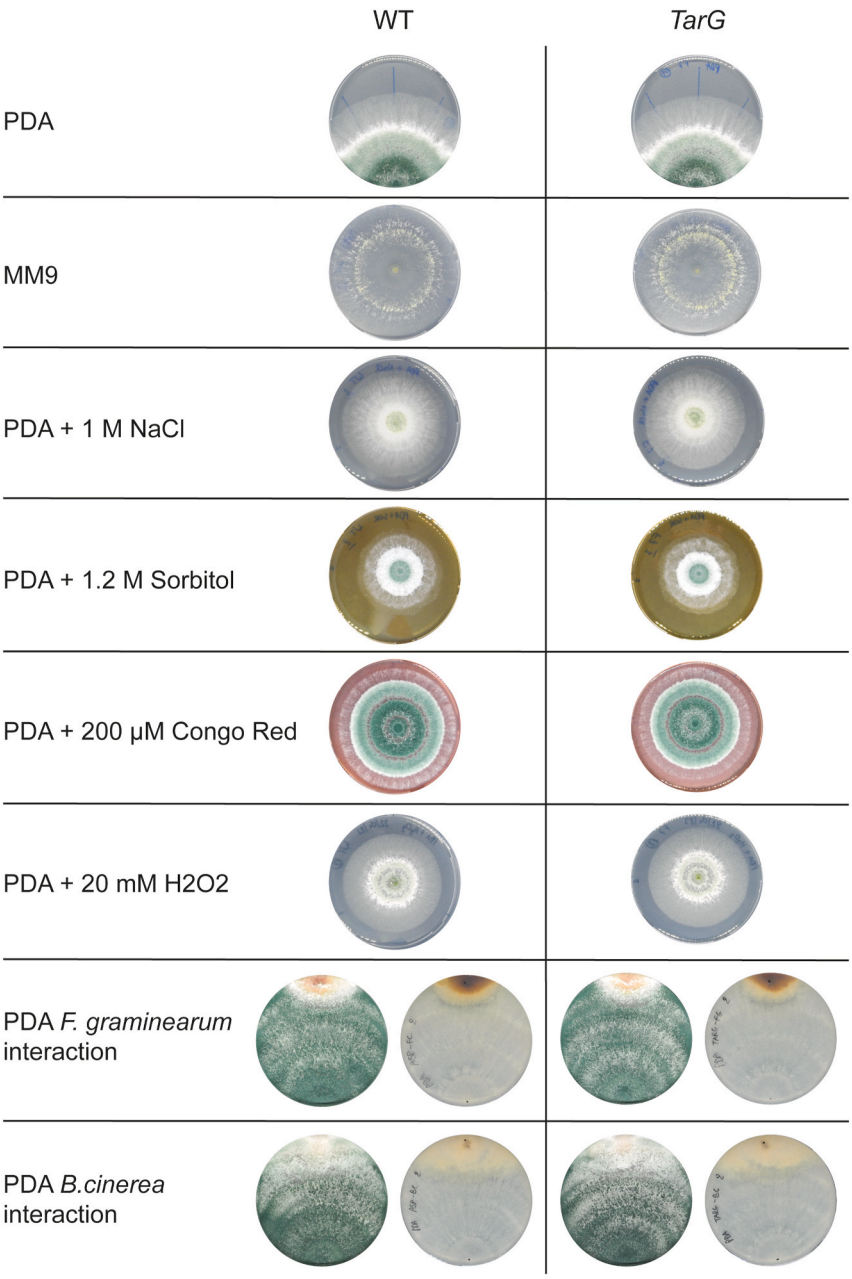

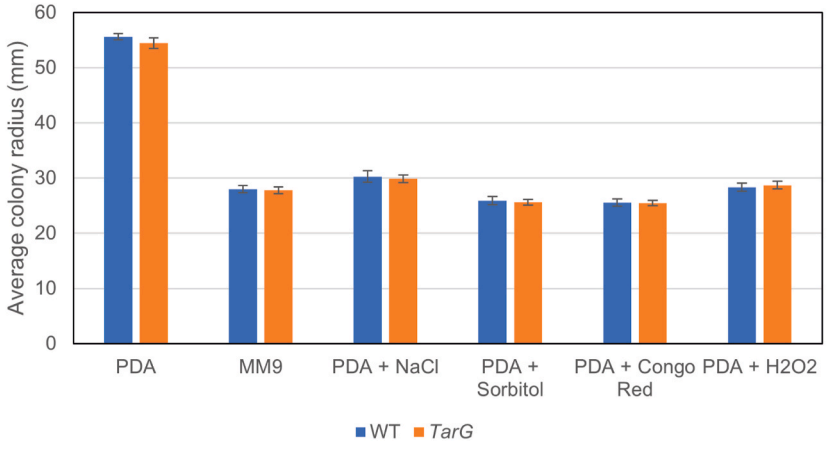

(caption on next page)

Fig. 1. Growth and interaction assays comparing the *T. asperellum* Grx1-roGFP2-expressing transformant strain (*TarG*) with *T. asperellum* wild-type (WT). The growth assays monitored fungal growth on PDA, MM9, PDA with 1 M NaCl, PDA with 1.2 M sorbitol, PDA with 200 μM congo red and PDA with 20 mM H_2O_2. The interaction assays were performed with *F. graminearum* or *B. cinerea* as hosts. For each growth assay, a representative colony is shown to assess colony morphology after four days of cultivation. The colony radius was measured and the resulting bar plot shows the average colony radius (n = three replicates) after three days of growth for MM9 and PDA with 200 μM congo red, and four days of growth for PDA, PDA with 1 M NaCl, PDA with 1.2 M sorbitol and PDA with 20 mM H_2O_2. For the interaction assays, both the top and bottom of one representative interaction is shown after seven days of cultivation. No significant differences were observed. (For interpretation of the references to colour in this figure legend, the reader is referred to the Web version of this article.)

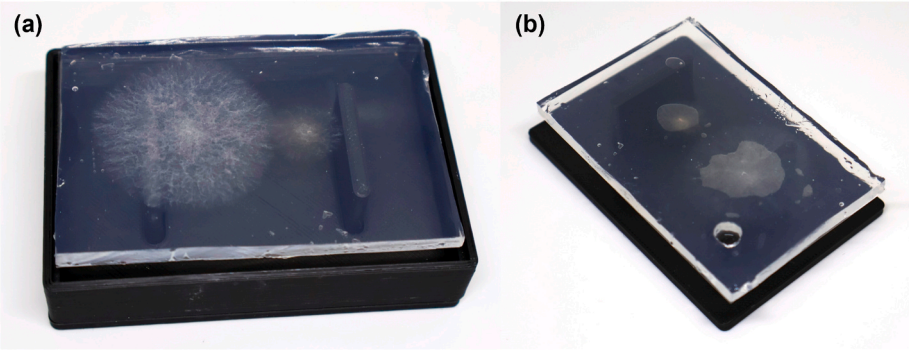

Fig. 2. Inncelly® basic chamber (ib02) used for incubation and preparation of the cultures for live-cell imaging analysis. The glass slide with medium is pushed out of the chamber in (a) and contains a dual-confrontation between the *T. asperellum* Grx1-roGFP2-expressing transformant strain (left) and *F. graminearum* (right). A glass slide was placed on top, the sample inverted, the bottom glass slide removed and a 5 mm circular well was made for *in situ* calibration (b).

F. graminearum) on the medium. The chambers were incubated for 44 h. Upon preparation for confocal imaging, the glass cover slip with the fungal culture was gently pushed out of the chamber using the associated stamp plate. Next, 50 μL of 0.9 % NaCl solution was applied to the growth front of the hyphal colony and a second glass cover slip was placed on top. Subsequently, the sample was inverted and the bottom glass cover slip was carefully removed. Finally, a 5 mm diameter circular well was made next to the growth front to allow addition of calibration solutions (Fig. 2, b). Before imaging dual confrontation cultures, an *in situ* calibration was established. To allow consistency and standardization throughout the experiments, this calibration was repeated for each dual confrontation and mycotoxin exposure sample. *In situ* calibration was achieved by first adding 50 μL of either a 100 mM or a 500 mM H_2O_2 solution and waiting until the roGFP2 signal reached a new steady state. Next, 100 μL of a 100 mM DTT solution was added. These concentrations are diluted by the presence of the 50 μL NaCl solution, resulting in a minimum of 50 mM or 250 mM H_2O_2 and 50 mM DTT actually experienced by the hyphae. Therefore, the minimum concentrations of 50 mM or 250 mM H_2O_2 and 50 mM DTT will be referred to hereafter.

Dual confrontation cultures were imaged for up to 30 min. Imaging was initiated shortly before *TarG* and *F. graminearum* entered physical interaction. Tip growth arrest was usually observed when the leading edge of the confronting fungal colonies approached within approximately 500 μm of each other. After imaging the confrontation, *in situ* calibration was performed for each sample.

The samples used for the mycotoxin exposure experiments, consisted of axenic *TarG* cultures prepared as described before but with the addition of two circular wells. To one well, deoxynivalenol (DON) or zearalenone (ZEN) solutions (dissolved in 10 % ethanol; Merck KGaA, Darmstadt, Germany) were added and the sample was imaged for up to 20 min. Afterwards, the opposite well was used for *in situ* calibration. DON and ZEN concentrations of 3.3 mM and 6.6 mM were used, with 50 μL solution added to the circular well. Once again, the presence of 50 μL NaCl solution resulted in a minimum of 1.65 mM DON and 3.3 mM ZEN experienced by the hyphae. Therefore, we will refer to 1.65 mM DON and 3.3 mM ZEN hereafter.

Samples as well as controls were imaged for a maximum of 30 min. The extended time of imaging did neither induce any considerable changes in the roGFP2 signal within the hyphae nor other stress morphologies (Supplementary Fig. S3). Furthermore, through past assessment of laser intensities and frequency of exposure that caused stress, we were able to stay below a laser intensity and frequency that could negatively affect the hyphae (data not shown).

2.5. Dual-excitation confocal ratiometric analysis

Using a custom MatLab (The MathWorks Inc. (2024). MATLAB version: 9.13.0 (R2024a), Natick, Massachusetts: The MathWorks Inc. https://www.mathworks.com) program (available on request from M.D. F.; Fricker, 2016; Samalova et al., 2014), the dual-excitation time series were processed and the ratio of fluorescence emissions was calculated. This ratio provides a quantitative measure of the redox potential of the Grx1-roGFP2 reporter within the hyphae, thus reflecting the glutathione redox potential (Schwarzländer et al., 2016). Firstly, background subtraction was performed to eliminate any non-specific fluorescence signals. To visualize changes in redox potential across the entire field of view, ratio images were generated by dividing the normalized fluorescence intensity values obtained with 405 nm excitation by those obtained with 488 nm excitation on a pixel-by-pixel basis (I_{405}/I_{488}). The resulting ratio image provides a spatial map of redox dynamics within the hyphae, with regions of higher ratio values corresponding to more oxidized cellular compartments and vice versa.

For pseudo-colour display, we encoded the masked ratio using hue on a spectral colour scale ranging from blue (most reduced) to red (most oxidized). The scale limits were deduced from the *in situ* calibration (described above in 'Live-cell imaging of dual confrontation and mycotoxin exposure'). The application of H_2O_2 followed by DTT drove Grx1-roGFP2 into highly oxidized and reduced forms, respectively. Finally, the ratio data for a specific region of interest were converted to the degree of oxidation ($OxD_{Grx1\text{-}roGFP2}$) following the approach outlined by Schwarzländer et al. (2008). Metadata for these analyses can be found in the supplementary data (Table S3).

3. Results

3.1. Grx1-roGFP2 reports glutathione redox potential in T. asperellum

We successfully integrated the genetic information of the Grx1-roGFP2 reporter into the genome of *T. asperellum*, resulting in transformant strain *TarG*. *TarG* also expresses the CRIB motif attached to the

fluorescent protein TagRFP-T (Fig. 3; e1, e2). Through a process of *in situ* calibration using 50 mM or 250 mM H_2O_2 and 50 mM DTT added externally, we were able to confirm reliable performance of the Grx1-roGFP2 probe within the newly established transformant strain. Fig. 3 shows a hypha exposed to 50 mM H_2O_2 and 50 mM DTT (Fig. 3, a1-e1) and a hypha exposed to 250 mM H_2O_2 and 50 mM DTT (Fig. 3, a2-e2). Grx1-roGFP2 showed consistent changes in its excitation spectrum as a result of H_2O_2 and DTT exposure. Upon exposure to oxidizing conditions (H_2O_2), the cysteine residues of Grx1-roGFP2 undergo reversible oxidation, leading to increased excitation at 405 nm and decreased excitability at 488 nm (Fig. 3; b1&2, c1&2, f1&2, g1&2). Conversely, under reducing conditions (DTT), the cysteine residues are reduced back to their original state, restoring the excitation profile, with more prominent excitability at 488 nm (Fig. 3; b1&2, c1&2, f1&2, g1&2). Exposure to 50 mM H_2O_2 resulted in an initial peak in the 405/488 nm ratio (Fig. 3; d1, h1) but did not lead to full oxidation of all Grx1-roGFP2 molecules (Fig. 3; i1). At this H_2O_2 concentration, the peak was quickly followed by a new steady state in the roGFP2 ratio which slowly decreased overtime. Through addition of 50 mM DTT, the ratio signal rapidly returned to starting values. Upon exposure to 250 mM H_2O_2 however, the roGFP2 ratio peaked and then proceeded to further increase instead of decreasing (Fig. 3; d2, h2). At this H_2O_2 concentration, the ratio reached the highest values we observed throughout our calibrations and therefore we define this as the ratio where 100 % of the Grx1-roGFP2 molecules are oxidized (Fig. 3; h2, i2). The ratio could only be brought back down to starting values through addition of DTT. The

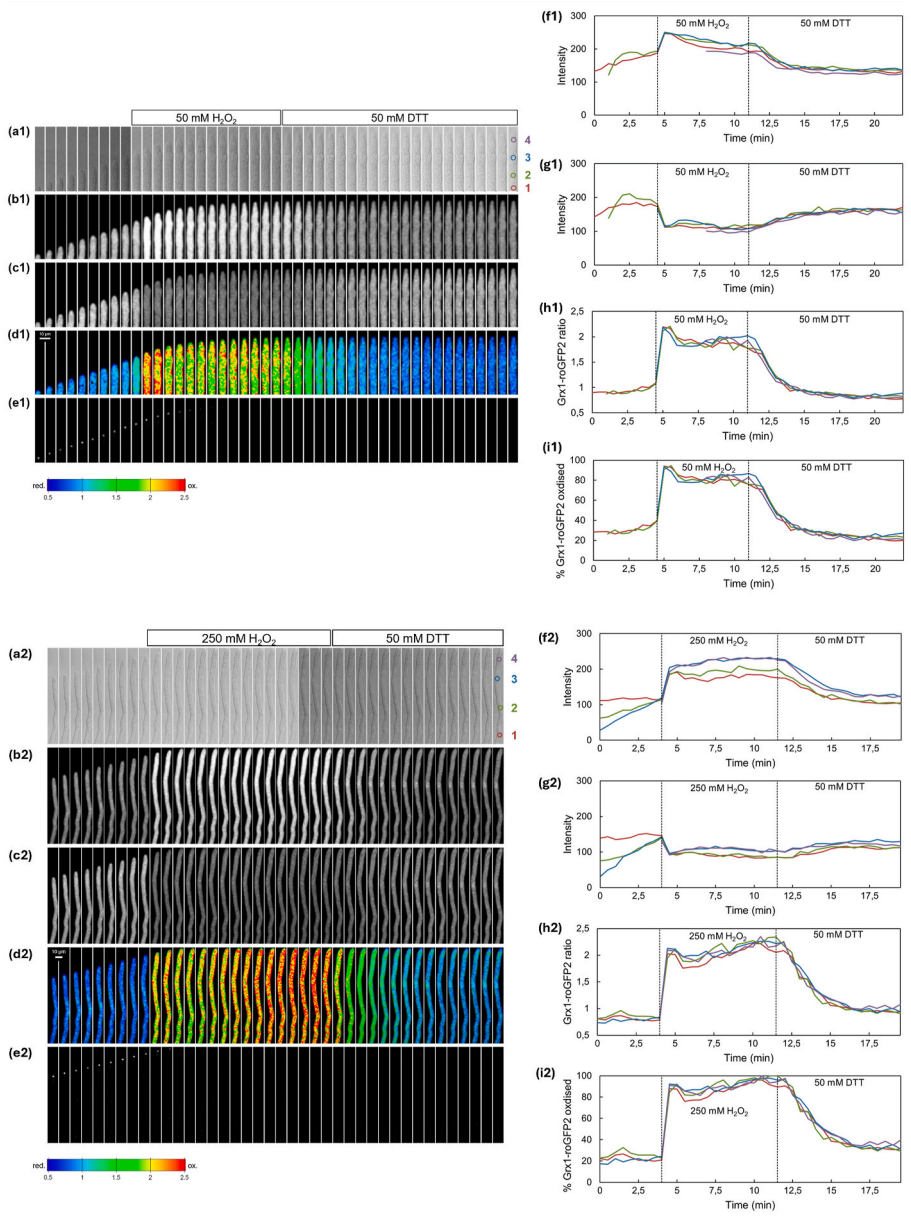

Fig. 3. Measurement of the glutathione redox potential of the glutathione pool in the *T. asperellum* Grx1-roGFP2-expressing transformant strain (*TarG*) during *in situ* calibration. *TarG* hyphae (a1, a2) were sequentially imaged with excitation at 405 nm (b1, b2) and 488 nm (c1, c2) at 30-s time intervals. The top hypha was imaged for 22 min and the bottom hypha was imaged for 19.5 min. After exposure of the hyphae to 50 mM H_2O_2 (top) or 250 mM H_2O_2 (bottom) followed by addition of 50 mM DTT, the degree of oxidation of Grx1-roGFP2 was visualized from the pseudo-colour-coded ratio (d1, d2). Four regions of interest (evenly spaced throughout the hypha; a1, a2) were selected where the average fluorescence at 405 nm (f1, f2) and 488 nm (g1, g2) was measured. The corresponding ratio (h1, h2) and degree of oxidation ($OxD_{Grx1\text{-}roGFP2}$; i1, i2) were calculated. Tip growth arrest occurred soon after addition of H_2O_2 as indicated by the disappearance of the CRIB reporter fluorescence (e1, e2). Scale bar: 10 μm. Videos of the complete time series can be found in the supporting data (Video S1 and S2). (For interpretation of the references to colour in this figure legend, the reader is referred to the Web version of this article.)

dynamic range of the reporter in *T. asperellum* was ~4.7 (Table S3), consistent with values reported in other plant, animal and fungal systems (Gutscher et al., 2008; Meyer and Dick, 2010; Samalova et al., 2014; Schwarzländer et al., 2016), and the resting ratio before treatment indicates a highly reduced cytoplasmic glutathione redox potential.

At both H_2O_2 concentrations, tip growth arrest occurred soon after H_2O_2 addition as indicated by the disappearance of the CRIB reporter fluorescence (Fig. 3; e1, e2) and cessation of tip elongation. The sample calibrated with 50 mM H_2O_2 was imaged for 22 min and the sample calibrated with 250 mM H_2O_2 was imaged for 19.5 min. We note that the sensitivity of the reporter is defined by its mid-point potential with respect to the midpoint potential of the GSH/GSSG redox couple, whilst the speed of the response and specificity for GSH are enhanced by the activity of the coupled Grx1 enzyme. The amount of H_2O_2 added externally that is required to shift the internal glutathione redox potential will depend on penetration through the cell wall, the activity of ROS detoxification, and the rate of internal GSSG reduction.

3.2. Glutathione redox potential does not change during early-stage interaction with F. graminearum

After confirming reliable performance of the Grx1-roGFP2 reporter in *T. asperellum*, we monitored the glutathione redox dynamics within *TarG* during interaction with *F. graminearum*. Through preculturing in inncelly® basic chambers and exact timing of the confocal imaging, we were able to image the time frame in which *TarG* approached *F. graminearum* and started to penetrate the outer edges of the host fungus colony, i.e. pre-physical and early physical interaction. In Fig. 4, the data for two time series are shown where a *TarG* hypha approaches the *F. graminearum* colony and then arrests tip growth as indicated by the disappearance of CRIB reporter fluorescence (Fig. 4; e1, e2). We show a montage of the hypha approaching the *F. graminearum* colony (Fig. 4; a1-e1, a2-e2) and the corresponding graphs with the fluorescence intensity at 405 nm or 488 nm excitation and the calculated ratio (Fig. 4; f1-h1, f2-h2). Neither during the time in which the *T. asperellum* hyphae approach the *F. graminearum* colony, nor during the transition to tip growth arrest, did we observe any considerable change in the roGFP2 ratio (Fig. 4; h1, h2). Three more time series are provided in the supporting data (Fig. S4). Similarly, during further monitoring of *TarG* hyphae growing into the *F. graminearum* colony, thus entering early physical interaction, no considerable change in roGFP2 fluorescence was observed (Supplementary Fig. S5). We hence did not receive any indication that a change in the glutathione redox potential of *T. asperellum* occurs during the pre-physical or early physical interaction with *F. graminearum*. In the supporting data (Fig. S6), a calibration is given for both time series which confirms reliable performance of the Grx1-roGFP2 molecule.

3.3. F. graminearum mycotoxins do not induce detectable oxidative stress

F. graminearum mycotoxins DON and ZEN are linked to oxidative stress induction in plants and mammalian cells (De Nijs et al., 1997; Favero et al., 2018; Feng et al., 2022; Filek et al., 2019; Mishra et al., 2014; Waśkiewicz et al., 2014; Yoon et al., 2019). To identify the response of *T. asperellum* to these *F. graminearum*-derived metabolites, we subjected *TarG* to highly concentrated DON or ZEN and monitored the glutathione redox dynamics. In Fig. 5, the data for two time series are shown where a *TarG* hypha was subjected to either DON (Fig. 5;

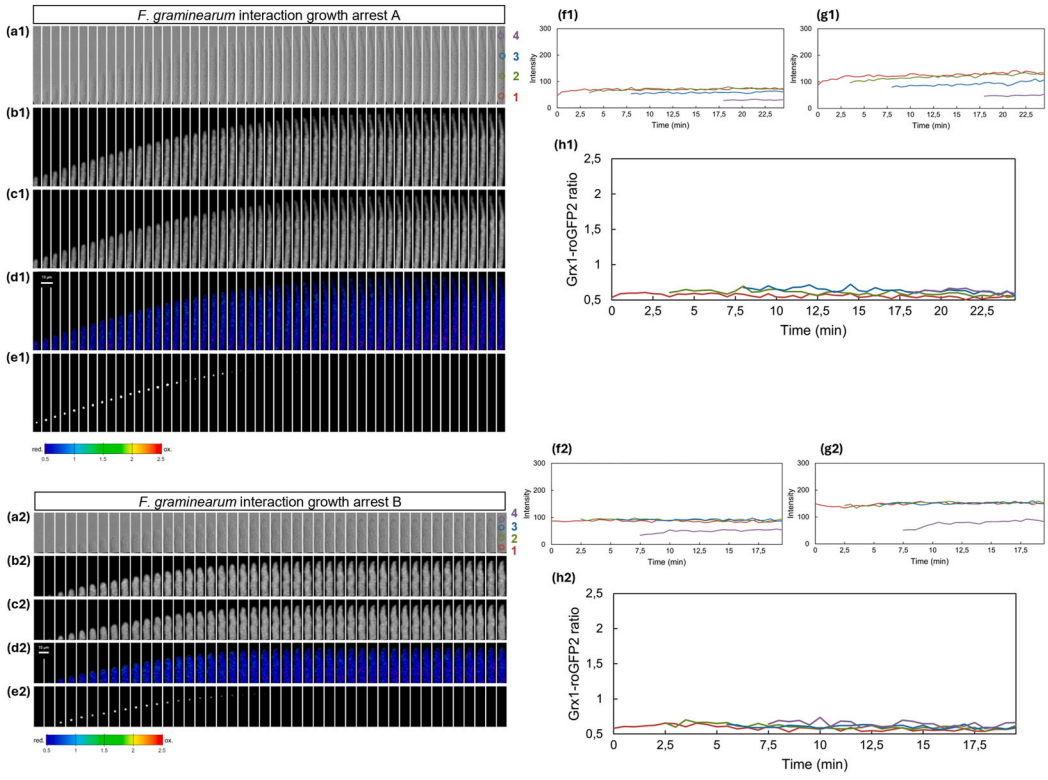

Fig. 4. Measurement of the glutathione redox potential of two individual hyphae of the *T. asperellum* Grx1-roGFP2-expressing transformant strain approaching a *F. graminearum* colony and arresting tip growth. The hyphae were sequentially imaged at 30-s intervals with excitation at 405 nm (b1, b2) and 488 nm (c1, c2). The top hypha was imaged for 19.5 min and the bottom hypha was imaged for 24.5 min. The degree of oxidation of Grx1-roGFP2 was visualized from the pseudo-colour-coded ratio (d1, d2). Four regions of interest (evenly spaced throughout the hypha; a1, a2) were selected where the average fluorescence at 405 nm (f1, f2) and 488 nm (g1, g2) was measured and the corresponding ratio (h1, h2) calculated. Tip growth arrest is indicated by the disappearance of the CRIB reporter fluorescence (e1, e2). Scale bar: 10 μm. Videos of the complete time series can be found in the supporting data (Video S3 and S4). (For interpretation of the references to colour in this figure legend, the reader is referred to the Web version of this article.)

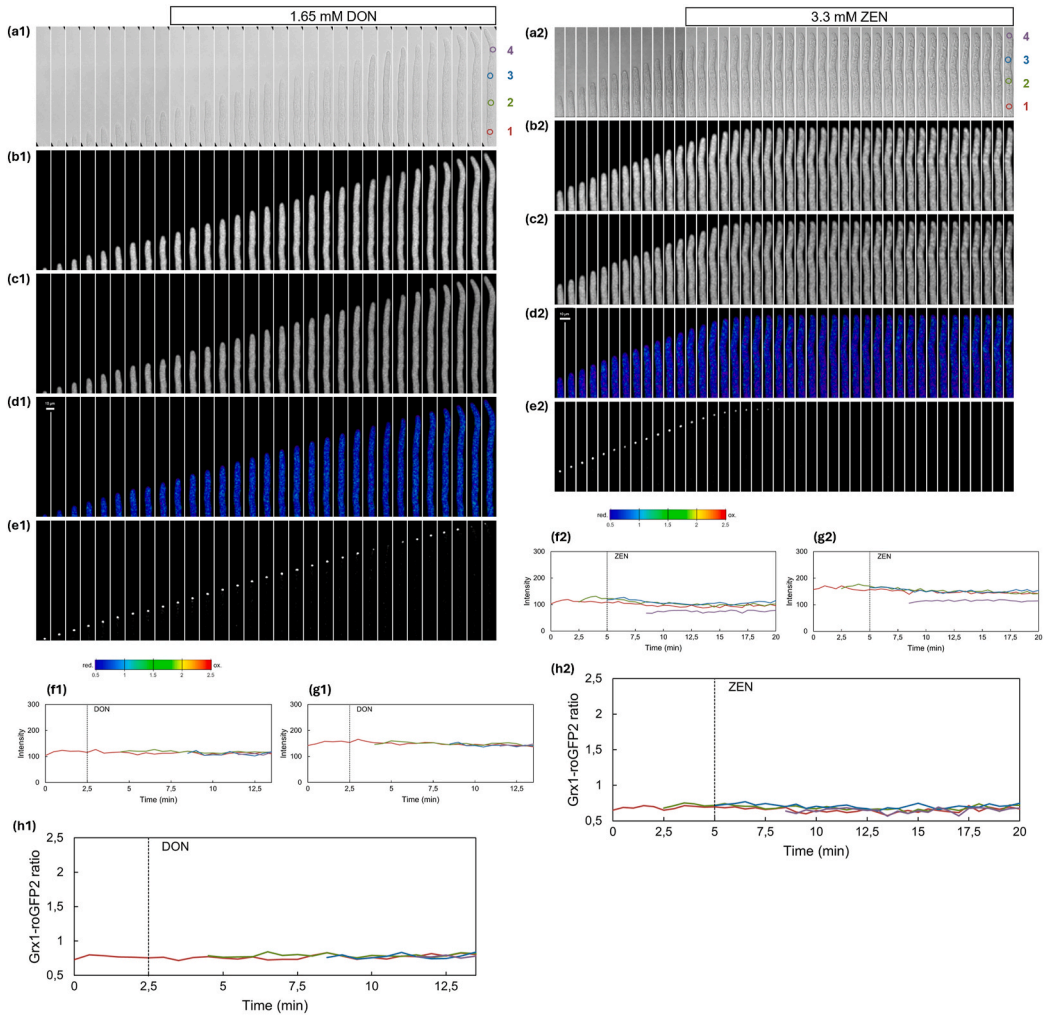

Fig. 5. Measurement of the glutathione redox potential of the glutathione pool in the *T. asperellum* Grx1-roGFP2-expressing strain (*TarG*) during mycotoxin exposure. *TarG* hyphae (a1, a2) were sequentially imaged with excitation at 405 nm (b1, b2) and 488 nm (c1, c2) at 30-s time intervals. The hypha subjected to DON was imaged for 14 min and the hypha subjected to ZEN was imaged for 20 min. After mycotoxin exposure, the degree of oxidation of Grx1-roGFP2 was visualized from the pseudo-colour-coded ratio (d1, d2). Four regions of interest (evenly spaced throughout the hypha; a1, a2) were selected where the average fluorescence at 405 nm (f1, f2) and 488 nm (g1, g2) was measured. The corresponding ratio (h1, h2) was calculated. Tip growth arrest occurred for the hypha subjected to ZEN but not for the hypha subjected to DON, as shown by the disappearance or presence of the CRIB reporter fluorescence, respectively (e1, e2). Scale bar: 10 μm. Videos of the complete time series can be found in the supporting data (Video S5 and S6). (For interpretation of the references to colour in this figure legend, the reader is referred to the Web version of this article.)

a1-h1) or ZEN (Fig. 5; a2-h2). A montage shows the hyphae (Fig. 5; a1-e1, a2-e2) and the corresponding graphs show average emission values at 405 nm or 488 nm excitation and the calculated ratio for four regions of interest (Fig. 5; f1-h1, f2-h2). Despite the use of up to 1.65 mM DON and 3.3 mM ZEN, we did not observe any indications of a change in the roGPF2 fluorescence emissions. DON exposure was imaged for 14 min and did not induce tip growth arrest, while ZEN exposure was imaged for 20 min and resulted in tip growth arrest as indicated by the disappearance of the CRIB reporter fluorescence (Fig. 5; e1, e2). Calibrations are shown in the supporting data (Fig. S6) which confirm reliable performance of the Grx1-roGFP2 molecule.

4. Discussion

In this study, we investigated glutathione redox dynamics within the mycoparasitic fungus *T. asperellum* through the use of the fluorescent reporter roGFP2. We aimed to demonstrate that Grx1-roGFP2 can be functionally expressed and used to analyse intracellular redox dynamics in real-time. Furthermore, we aimed to reveal whether Grx1-roGFP2 exhibits a dynamic response during the interaction between *T. asperellum* and a host fungus and whether hyphal tip growth arrest could be induced by intracellular ROS accumulation during this interaction. Finally, we investigated whether the *F. graminearum* mycotoxins DON and ZEN induce oxidative stress in *T. asperellum* as previously described for plants and mammalian cells (De Nijs et al., 1997; Favero et al., 2018; Feng et al., 2022; Filek et al., 2019; Mishra et al., 2014; Waśkiewicz et al., 2014; Yoon et al., 2019).

We used an electrotransformation approach to successfully integrate the Grx1-roGFP2-encoding construct into the genome of *T. asperellum* and showed that this fluorescent probe is functionally expressed in *T. asperellum* hyphae. Moreover, we simultaneously inserted the CRIB reporter system (Lichius et al., 2014; Moreno-Ruiz et al., 2021), resulting in a double fluorescent reporter strain allowing the monitoring of both the glutathione redox dynamics and growth behaviour of *T. asperellum*. In *T. reesei*, electroporation of fungal conidia as a genetic transformation approach is well established (Kim and Miasnikov, 2013; Schuster et al., 2012; Wanka, 2021). Compared with the classical protoplast transformation approach, electroporation tends to be less time-consuming and easier to perform while retaining a comparable efficiency (Schuster et al., 2012; Wanka, 2021). To our knowledge, this

study is the first that describes the successful application of electroporation to transform *T. asperellum*. Given the advantages of this approach, it will be useful to investigate its application in other *Trichoderma* spp. and optimize it to integrate novel genomic engineering tools such as CRISPR-Cas9 (Wang et al., 2022).

Considering the putative significance of ROS during the mycoparasitic interaction, it is crucial to expand our methodological repertoire to study this topic. The development of the roGFP2 reporter system in *T. asperellum* has enabled us to investigate glutathione redox dynamics in this key biocontrol fungus. *TarG* was subjected to interaction with *F. graminearum* to improve our understanding of the antioxidant defence system within *T. asperellum* and its role during the mycoparasitic interaction. Following the successful application of roGFP2 in *B. cinerea* and *M. oryzae* (Heller et al., 2012; Samalova et al., 2014), we are the first to apply this probe in a mycoparasitic fungus. Moreover, the Grx1-roGFP2 reporter and the CRIB reporter system were co-expressed in the same fungus resulting in a reporter strain that allows us to link glutathione redox dynamics within the hyphae to growth activity at the front of the fungal colony. In future glutathione redox assays where the parameter of active tip growth holds significant value and tip growth arrest is difficult to detect, the additional CRIB reporter could provide essential information on the growth behaviour of the hyphae.

Through application of Grx1-roGFP2 in *T. asperellum*, unique insights into the real-time glutathione redox dynamics within this important biocontrol agent were obtained. For *in situ* calibration, *TarG* was subjected to highly concentrated H_2O_2 and DTT. Upon addition of 50 mM H_2O_2 externally, we observed an initial peak in the 405/488 nm ratio, indicating maximal roGFP2 oxidation. At this concentration, however, the hyphae appear to be partially able to mitigate the oxidative loads as indicated by the 405/488 nm ratio returning to a lower plateau after some minutes. Strikingly, an external concentration of 250 mM H_2O_2 was required to induce and maintain a maximally oxidized glutathione pool. Upon comparison with plant or HeLa cells, where H_2O_2 concentrations of less than 1 mM are sufficient to induce near complete oxidation of roGFP2 (Hanson et al., 2004; Meyer et al., 2007), it becomes apparent that the antioxidant capacity of *T. asperellum* is vastly greater, indicating a robust antioxidant defence system. These findings are in agreement with Morán-Diez et al. (2021), who suggested that high tolerance to ROS is a peculiarity of *Trichoderma* spp. that facilitates their biocontrol activity against phytopathogens. Nevertheless, similar tolerance to high levels of H_2O_2 have also been reported for the phytopathogenic fungi *B. cinerea* (Heller et al., 2012) and *M. oryzae* (Samalova et al., 2014), suggesting that robust anti-oxidant defences are widespread in fungi. At this stage we cannot determine whether the tolerance to high external H_2O_2 is achieved through reduced permeability of the cell wall, high level of ROS detoxification systems and/or the ability to rapidly reduce oxidized GSSG, but the physiological consequence is that *T. asperellum* is remarkably resistant to externally imposed oxidative loads.

Monitoring the Grx1-roGFP2 signal during mycoparasitic interaction of *TarG* with *F. graminearum* further confirmed the effective antioxidant system of *T. asperellum*. Our current understanding of mycoparasitic interactions suggests that the mycoparasite experiences considerable oxidative loads during the interaction (Druzhinina et al., 2011; Morán-Diez et al., 2021; Waśkiewicz et al., 2014). Nevertheless, extended monitoring of the roGFP2 signal in *T. asperellum* being confronted with the fungal host, revealed no considerable changes in glutathione oxidation during any stage of the interaction. Thus, we hypothesize that the *T. asperellum* antioxidant defence system is able to rapidly mitigate any oxidative loads experienced during the mycoparasitic interaction, an ability which could facilitate the efficient parasitism of other fungi in its environment, as previously hypothesized by Morán-Diez et al. (2021).

The obtained data evidence that tip growth arrest of the *Trichoderma* hyphae at the interaction zone is not the result of extensive intracellular glutathione oxidation. Considering the major role of glutathione in the antioxidant defence system of eukaryotes, we conclude that hyphal tip growth arrest is unlikely to be induced by significant increases in the overall oxidative stress experienced by the hyphal cells. Together with a rapidly acting antioxidant defence system, *T. asperellum* likely developed other signalling pathways that induce tip growth arrest before intracellular ROS concentrations exceed its antioxidant capacity. As the Grx1-roGFP2 reporter only monitors the glutathione redox potential (Schwarzländer et al., 2016), it is perfectly possible that redox signalling involves shifts in the redox potential of other redox couples or lipid oxidation, potentially causing hyphal tip growth arrest.

The *F. graminearum* mycotoxins DON and ZEN have previously been shown to induce oxidative stress in plant and mammalian cells (Filek et al., 2019; Mishra et al., 2014; Waśkiewicz et al., 2014; Yoon et al., 2019). There, DON and ZEN concentrations of 50 μM and 126 μM, respectively, represent the upper limit of what is required to connect these mycotoxins to oxidative stress induction (Filek et al., 2019; Shieh et al., 2021; Wang et al., 2020; Xu et al., 2024; Yoon et al., 2019). In our study, the glutathione-related antioxidant defence system of *T. asperellum* remained untriggered even at extremely high DON and ZEN concentrations of 1.65 mM and 3.3 mM, respectively. Although hyphal tip growth arrest during ZEN exposure was observed, the absence of glutathione oxidation inside the fungal hyphae evidences a robust antioxidant defence system in *T. asperellum*. Our findings do not exclude shifts in the redox potential of other redox couples or lipid oxidation, but the absence of glutathione oxidation indicate that the mycotoxins could exert cytotoxic effects on *T. asperellum* through a mechanism that does not lead to intracellular ROS accumulation and thus is completely different from what takes place in plant or mammalian cells (Favero et al., 2018; Feng et al., 2022; Filek et al., 2019; Mishra et al., 2014).

Our study has successfully laid the foundation for further investigation into the oxidative stress response in *Trichoderma* spp. through live-cell imaging. Understanding how *Trichoderma* species cope with oxidative loads is crucial to harnessing their full potential. Future investigations could use this dual-reporter system to investigate glutathione redox dynamics at the germling level to improve our understanding of how mature colonies establish and which environmental stressors could hinder colony establishment. Furthermore, the Grx1-roGFP2 probe could be applied to mutants of *Trichoderma* spp. deficient in pathways related to oxidative stress responses such as mutants unable to recycle oxidized glutathione (GSSG). Additionally, this dual-reporter system can be applied in other *Trichoderma* spp. such as *T. virens, T. atroviride* and *T. harzianum* in order to compare the degree of resistance to oxidative loads between these mycoparasites and investigate differences in resistance to oxidative loads upon interaction with fungal hosts. Investigating oxidative responses during the mycoparasitic interaction allows us to better understand the role of ROS in the antagonism and defence by *Trichoderma* and its host. The knowledge generated through the use of Grx1-roGFP2 as a reporter system may pave the way towards increased appreciation for how oxidative stress tolerance shapes the mycoparasitic interaction.

CRediT authorship contribution statement

Siebe Pierson: Writing – original draft, Visualization, Validation, Methodology, Investigation, Formal analysis, Data curation, Conceptualization. **Mark Fricker:** Writing – review & editing, Supervision, Software, Methodology, Formal analysis, Conceptualization. **Alexander Lichius:** Writing – review & editing, Supervision, Methodology, Conceptualization. **Adolf Michael Sandbichler:** Writing – review & editing, Methodology, Investigation. **Susanne Zeilinger:** Writing – review & editing, Supervision, Resources, Project administration, Funding acquisition, Conceptualization.

Declaration of competing interest

The authors declare that they have no known competing financial

interests or personal relationships that could have appeared to influence the work reported in this paper.

Acknowledgements

We would like to thank Markus Schwarzländer for providing the pBinCM-GRX1-roGFP2 plasmid. We acknowledge the DK program Bio-App (University of Innsbruck) for funding. This article is part of the special issue for the V International Symposium on Fungal Stress (ISFUS), supported by the Coordenação de Aperfeiçoamento de Pessoal de Nível Superior (CAPES) grant 88881.942500/2024-01.

Appendix A. Supplementary data

Supplementary data to this article can be found online at https://doi.org/10.1016/j.funbio.2025.101549.

References

Aguirre, J., Hansberg, W., Navarro, R., 2006. Fungal responses to reactive oxygen species. Med. Mycol. 44 (Suppl. ment_1), S101–S107. https://doi.org/10.1080/13693780600900080.

Ahmad, P., Hashem, A., Abd-Allah, E.F., Alqarawi, A.A., John, R., Egamberdieva, D., Gucel, S., 2015. Role of *Trichoderma harzianum* in mitigating NaCl stress in Indian mustard (*Brassica juncea* L) through antioxidative defense system. Front. Plant Sci. 6, 868. https://doi.org/10.3389/fpls.2015.00868.

Aquilano, K., Baldelli, S., Ciriolo, M.R., 2014. Glutathione: new roles in redox signaling for an old antioxidant. Front. Pharmacol. 5. https://doi.org/10.3389/fphar.2014.00196.

Barnett, H.L., 1963. The nature of mycoparasitism by fungi. Annu. Rev. Microbiol. 17 (1), 1–14. https://doi.org/10.1146/annurev.mi.17.100163.000245.

Belozerskaya, T.A., Gessler, N.N., 2007. Reactive oxygen species and the strategy of antioxidant defense in fungi: a review. Appl. Biochem. Microbiol. 43 (5), 506–515. https://doi.org/10.1134/S0003683807050031.

Boonstra, J., Post, J.A., 2004. Molecular events associated with reactive oxygen species and cell cycle progression in mammalian cells. Gene 337, 1–13. https://doi.org/10.1016/j.gene.2004.04.032.

Chen, S., Yan, Y., Wang, Y., Wu, M., Mao, Q., Chen, Y., Ren, J., Liu, A., Lin, X., Ahammed, G.J., 2020. *Trichoderma asperellum* reduces phoxim residue in roots by promoting plant detoxification potential in *Solanum lycopersicum* L. Environ. Pollut. 259, 113893. https://doi.org/10.1016/j.envpol.2019.113893.

Chen, S.-C., Ren, J.-J., Zhao, H.-J., Wang, X.-L., Wang, T.-H., Jin, S.-D., Wang, Z.-H., Li, C., Liu, A.-R., Lin, X.-M., Ahammed, G.J., 2019. *Trichoderma harzianum* improves defense against *Fusarium oxysporum* by regulating ROS and RNS metabolism, redox balance, and energy flow in cucumber roots. Phytopathology 109 (6), 972–982. https://doi.org/10.1094/PHYTO-09-18-0342-R.

Chuffart, F., Yvert, G., 2014. MyLabStocks: a web-application to manage molecular biology materials. Yeast 31 (5), 179–184. https://doi.org/10.1002/yea.3008.

Contreras-Cornejo, H.A., Schmoll, M., Esquivel-Ayala, B.A., González-Esquivel, C.E., Rocha-Ramírez, V., Larsen, J., 2024. Mechanisms for plant growth promotion activated by *Trichoderma* in natural and managed terrestrial ecosystems. Microbiol. Res. 281, 127621. https://doi.org/10.1016/j.micres.2024.127621.

De Nijs, M., Van Egmond, H.p., Rombouts, F.m., Notermans, S.h. w., 1997. Identification of hazardous *Fusarium* secondary metabolites occurring in food raw materials. J. Food Saf. 17 (3), 161–191. https://doi.org/10.1111/j.1745-4565.1997.tb00185.x.

Di Meo, S., Reed, T.T., Venditti, P., Victor, V.M., 2016. Role of ROS and RNS sources in physiological and pathological conditions. Oxid. Med. Cell. Longev., e1245049 https://doi.org/10.1155/2016/1245049, 2016.

Dooley, C.T., Dore, T.M., Hanson, G.T., Jackson, W.C., Remington, S.J., Tsien, R.Y., 2004. Imaging dynamic redox changes in mammalian cells with green fluorescent protein indicators. J. Biol. Chem. 279 (21), 22284–22293. https://doi.org/10.1074/jbc.M312847200.

Druzhinina, I.S., Seidl-Seiboth, V., Herrera-Estrella, A., Horwitz, B.A., Kenerley, C.M., Monte, E., Mukherjee, P.K., Zeilinger, S., Grigoriev, I.V., Kubicek, C.P., 2011. *Trichoderma*: the genomics of opportunistic success. Nat. Rev. Microbiol. 9 (10), 749–759. https://doi.org/10.1038/nrmicro2637.

Ernesto Juniors, P.-T., Valeria, C.-L., Santiago, P.-O., Mario, R.-M., Gabriela, S.-J., 2020. Tolerance to oxidative stress caused by copper (Cu) in *Trichoderma asperellum* to. Biocatal. Agric. Biotechnol. 29, 101783. https://doi.org/10.1016/j.bcab.2020.101783.

Favero, G., Woelflingseder, L., Braun, D., Puntscher, H., Kütt, M.-L., Dellafiora, L., Warth, B., Pahlke, G., Dall'Asta, C., Adam, G., Marko, D., 2018. Response of intestinal HT-29 cells to the trichothecene mycotoxin deoxynivalenol and its sulfated conjugates. Toxicol. Lett. 295. https://doi.org/10.1016/j.toxlet.2018.07.007.

Feng, Y.-Q., Zhao, A.-H., Wang, J.-J., Tian, Y., Yan, Z.-H., Dri, M., Shen, W., De Felici, M., Li, L., 2022. Oxidative stress as a plausible mechanism for zearalenone to induce genome toxicity. Gene 829, 146511. https://doi.org/10.1016/j.gene.2022.146511.

Filek, M., Sieprawska, A., Kościelniak, J., Oklestkova, J., Jurczyk, B., Telk, A., Biesaga-Kościelniak, J., Janeczko, A., 2019. The role of chloroplasts in the oxidative stress that is induced by zearalenone in wheat plants – the functions of 24-epibrassinolide and selenium in the protective mechanisms. Plant Physiol. Biochem. 137, 84–92. https://doi.org/10.1016/j.plaphy.2019.01.030.

Fricker, M.D., 2016. Quantitative redox imaging software. Antioxidants Redox Signal. 24 (13), 752–762. https://doi.org/10.1089/ars.2015.6390.

Gao, J., Wang, Q., Sun, J., He, A., Chen, J., 2018. Biological role of the superoxide dismutase TaSOD on vegetative growth, stress response, and antagonism in *Trichoderma asperellum*. Australas. Plant Pathol. 47 (6), 623–627. https://doi.org/10.1007/s13313-018-0605-5.

Gessler, N.N., Aver'yanov, A.A., Belozerskaya, T.A., 2007. Reactive oxygen species in regulation of fungal development. Biochemistry. Biokhimiia 72 (10), 1091–1109. https://doi.org/10.1134/s0006297907100070.

Goswami, R.S., Kistler, H.C., 2004. Heading for disaster: *Fusarium graminearum* on cereal crops. Mol. Plant Pathol. 5 (6), 515–525. https://doi.org/10.1111/j.1364-3703.2004.00252.x.

Gutscher, M., Pauleau, A.-L., Marty, L., Brach, T., Wabnitz, G.H., Samstag, Y., Meyer, A. J., Dick, T.P., 2008. Real-time imaging of the intracellular glutathione redox potential. Nat. Methods 5 (6), 553–559. https://doi.org/10.1038/nmeth.1212.

Guzmán-Guzmán, P., Kumar, A., de los Santos-Villalobos, S., Parra-Cota, F.I., Orozco-Mosqueda, Ma del C., Fadiji, A.E., Hyder, S., Babalola, O.O., Santoyo, G., 2023. *Trichoderma* species: our best fungal allies in the biocontrol of plant. Diseases—A Rev. Plants 12 (3), 432. https://doi.org/10.3390/plants12030432.

Hanson, G.T., Aggeler, R., Oglesbee, D., Cannon, M., Capaldi, R.A., Tsien, R.Y., Remington, S.J., 2004. Investigating mitochondrial redox potential with redox-sensitive green fluorescent protein indicators. J. Biol. Chem. 279 (13), 13044–13053. https://doi.org/10.1074/jbc.M312846200.

Heller, J., Meyer, A.J., Tudzynski, P., 2012. Redox-sensitive GFP2: use of the genetically encoded biosensor of the redox status in the filamentous fungus *Botrytis cinerea*. Mol. Plant Pathol. 13 (8), 935–947. https://doi.org/10.1111/j.1364-3703.2012.00802.x.

Heller, J., Tudzynski, P., 2011. Reactive oxygen species in phytopathogenic fungi: signaling, development, and disease. Annu. Rev. Phytopathol. 49 (1), 369–390. https://doi.org/10.1146/annurev-phyto-072910-095355.

Hernández-Oñate, M.A., Esquivel-Naranjo, E.U., Mendoza-Mendoza, A., Stewart, A., Herrera-Estrella, A.H., 2012. An injury-response mechanism conserved across kingdoms determines entry of the fungus *Trichoderma atroviride* into development. Proc. Natl. Acad. Sci. USA 109 (37), 14918–14923. https://doi.org/10.1073/pnas.1209396109.

Jansen, C., von Wettstein, D., Schäfer, W., Kogel, K.-H., Felk, A., Maier, F.J., 2005. Infection patterns in barley and wheat spikes inoculated with wild-type and trichodiene synthase gene disrupted *Fusarium graminearum*. Proc. Natl. Acad. Sci. USA 102 (46), 16892–16897. https://doi.org/10.1073/pnas.0508467102.

Karlsson, M., Atanasova, L., Jensen, D.F., Zeilinger, S., 2017. Necrotrophic mycoparasites and their genomes. Microbiol. Spectr. 5 (2). https://doi.org/10.1128/microbiolspec.funk-0016–2016, 10.1128/microbiolspec.funk-0016-2016.

Kim, S., Miasnikov, A., 2013. *Method for introducing nucleic acids into fungal cells* (United States Patent US8450098B2). https://patents.google.com/patent/US8450098B2/en.

Kuczler, M.D., Olseen, A.M., Pienta, K.J., Amend, S.R., 2021. ROS-induced cell cycle arrest as a mechanism of resistance in polyaneuploid cancer cells (PACCs). Prog. Biophys. Mol. Biol. 165, 3–7. https://doi.org/10.1016/j.pbiomolbio.2021.05.002.

Lichius, A., Goryachev, A.B., Fricker, M.D., Obara, B., Castro-Longoria, E., Read, N.D., 2014. CDC-42 and RAC-1 regulate opposite chemotropisms in Neurospora crassa. J. Cell Sci. 127 (Pt 9), 1953–1965. https://doi.org/10.1242/jcs.141630.

Lichius, A., Read, N., 2009. A versatile set of Lifeact-RFP expression plasmids for live-cell imaging of F-actin in filamentous fungi. Fungal Genetics Report 57. https://doi.org/10.4148/1941-4765.1070.

Mastouri, F., Björkman, T., Harman, G.E., 2012. *Trichoderma harzianum* enhances antioxidant defense of tomato seedlings and resistance to water deficit. Mol. Plant Microbe Interact.: MPMI (Mol. Plant-Microbe Interact.) 25 (9), 1264–1271. https://doi.org/10.1094/MPMI-09-11-0240.

Meng, L., Mestdagh, H., Ameye, M., Audenaert, K., Höfte, M., Van Labeke, M.-C., 2020. Phenotypic variation of *Botrytis cinerea* isolates is influenced by spectral light quality. Front. Plant Sci. 11. https://doi.org/10.3389/fpls.2020.01233.

Mentges, M., Bormann, J., 2015. Real-time imaging of hydrogen peroxide dynamics in vegetative and pathogenic hyphae of *Fusarium graminearum*. Sci. Rep. 5 (1), 14980. https://doi.org/10.1038/srep14980.

Meyer, A.J., 2008. The integration of glutathione homeostasis and redox signaling. J. Plant Physiol. 165 (13), 1390–1403. https://doi.org/10.1016/j.jplph.2007.10.015.

Meyer, A.J., Brach, T., Marty, L., Kreye, S., Rouhier, N., Jacquot, J.-P., Hell, R., 2007. Redox-sensitive GFP in *Arabidopsis thaliana* is a quantitative biosensor for the redox potential of the cellular glutathione redox buffer. Plant J. 52 (5), 973–986. https://doi.org/10.1111/j.1365-313X.2007.03280.x.

Meyer, A.J., Dick, T.P., 2010. Fluorescent protein-based redox probes. Antioxidants Redox Signal. 13 (5), 621–650. https://doi.org/10.1089/ars.2009.2948.

Mishra, S., Dwivedi, P.D., Pandey, H.P., Das, M., 2014. Role of oxidative stress in Deoxynivalenol induced toxicity. Food Chem. Toxicol. 72, 20–29. https://doi.org/10.1016/j.fct.2014.06.027.

Montero-Barrientos, M., Hermosa, R., Cardoza, R.E., Gutiérrez, S., Monte, E., 2011. Functional analysis of the *Trichoderma harzianum* nox 1 gene, encoding an NADPH oxidase, relates production of reactive oxygen species to specific biocontrol activity against *Pythium ultimum*. Appl. Environ. Microbiol. 77 (9), 3009–3016. https://doi.org/10.1128/AEM.02486-10.

Morán-Diez, M.E., Martínez de Alba, Á.E., Rubio, M.B., Hermosa, R., Monte, E., 2021. *Trichoderma* and the plant heritable priming responses. J. Fungi 7 (4), 318. https://doi.org/10.3390/jof7040318.

Moreno-Ruiz, D., Lichius, A., Turrà, D., Di Pietro, A., Zeilinger, S., 2020. Chemotropism assays for plant symbiosis and mycoparasitism related compound screening in

Trichoderma atroviride. Front. Microbiol. 11, 601251. https://doi.org/10.3389/fmicb.2020.601251.
Moreno-Ruiz, D., Salzmann, L., Fricker, M.D., Zeilinger, S., Lichius, A., 2021. Stress-activated protein kinase signalling regulates mycoparasitic hyphal-hyphal interactions in *Trichoderma atroviride*. J. Fungi 7 (5), 365. https://doi.org/10.3390/jof7050365.
Parry, D.W., Jenkinson, P., McLEOD, L., 1995. *Fusarium* ear blight (scab) in small grain cereals—a review. Plant Pathol. 44 (2), 207–238. https://doi.org/10.1111/j.1365-3059.1995.tb02773.x.
Riquelme, M., Martínez-Núñez, L., 2016. Hyphal ontogeny in *Neurospora crassa*: a model organism for all seasons. F1000Research 5, 2801. https://doi.org/10.12688/f1000research.9679.1.
Samalova, M., Meyer, A.J., Gurr, S.J., Fricker, M.D., 2014. Robust anti-oxidant defences in the rice blast fungus *Magnaporthe oryzae* confer tolerance to the host oxidative burst. New Phytol. 201 (2), 556–573. https://doi.org/10.1111/nph.12530.
Schuster, A., Bruno, K.S., Collett, J.R., Baker, S.E., Seiboth, B., Kubicek, C.P., Schmoll, M., 2012. A versatile toolkit for high throughput functional genomics with *Trichoderma reesei*. Biotechnol. Biofuels 5, 1. https://doi.org/10.1186/1754-6834-5-1.
Schwarzländer, M., Dick, T.P., Meyer, A.J., Morgan, B., 2016. Dissecting redox biology using fluorescent protein sensors. Antioxidants Redox Signal. 24 (13), 680–712. https://doi.org/10.1089/ars.2015.6266.
Schwarzländer, M., Fricker, M.D., Müller, C., Marty, L., Brach, T., Novak, J., Sweetlove, L.J., Hell, R., Meyer, A.J., 2008. Confocal imaging of glutathione redox potential in living plant cells. J. Microsc. 231 (2), 299–316. https://doi.org/10.1111/j.1365-2818.2008.02030.x.
Shieh, P., Hsu, S.-S., Liang, W.-Z., 2021. Mechanisms underlying protective effects of vitamin E against mycotoxin deoxynivalenol-induced oxidative stress and its related cytotoxicity in primary human brain endothelial cells. Environ. Toxicol. 36 (7), 1375–1388. https://doi.org/10.1002/tox.23133.
Sies, H., 1991. Oxidative stress: introduction. Oxidative Stress : Oxidan. Antioxid. 15–21.
Singh, Y., Nair, A.M., Verma, P.K., 2021. Surviving the odds: from perception to survival of fungal phytopathogens under host-generated oxidative burst. Plant Commun. 2 (3). https://doi.org/10.1016/j.xplc.2021.100142.
Tudzynski, P., Heller, J., Siegmund, U., 2012. Reactive oxygen species generation in fungal development and pathogenesis. Curr. Opin. Microbiol. 15 (6), 653–659. https://doi.org/10.1016/j.mib.2012.10.002.
Tyśkiewicz, R., Nowak, A., Ozimek, E., Jaroszuk-Ściseł, J., 2022. *Trichoderma*: the current status of its application in agriculture for the biocontrol of fungal phytopathogens and stimulation of plant growth. Int. J. Mol. Sci. 23 (4), 2329. https://doi.org/10.3390/ijms23042329.
Ukuwela, A.A., Bush, A.I., Wedd, A.G., Xiao, Z., 2018. Glutaredoxins employ parallel monothiol–dithiol mechanisms to catalyze thiol–disulfide exchanges with protein disulfides. Chem. Sci. 9 (5), 1173–1183. https://doi.org/10.1039/C7SC04416J.
Wang, Y., Chen, H., Ma, L., Gong, M., Wu, Y., Bao, D., Zou, G., 2022. Use of CRISPR-Cas tools to engineer *Trichoderma* species. Microb. Biotechnol. 15 (10), 2521–2532. https://doi.org/10.1111/1751-7915.14126.
Wang, Y., Yan, H., Wang, Q., Zheng, R., Xia, K., Liu, Y., 2020. Regulation of the phytotoxic response of *Arabidopsis thaliana* to the *Fusarium* mycotoxin deoxynivalenol. J. Integr. Agric. 19 (3), 759–767. https://doi.org/10.1016/S2095-3119(19)62741-3.
Wanka, F., 2021. Open the pores: electroporation for the transformation of *Trichoderma reesei*. In: Mach-Aigner, A.R., Martzy, R. (Eds.), Trichoderma Reesei: Methods and Protocols. Springer US, pp. 73–78. https://doi.org/10.1007/978-1-0716-1048-0_6.
Warris, A., Ballou, E.R., 2019. Oxidative responses and fungal infection biology. Semin. Cell Dev. Biol. 89, 34–46. https://doi.org/10.1016/j.semcdb.2018.03.004.
Waśkiewicz, A., Morkunas, I., Bednarski, W., Mai, V.C., Formela, M., Beszterda, M., Wiśniewska, H., Goliński, P., 2014. Deoxynivalenol and oxidative stress indicators in winter wheat inoculated with *Fusarium graminearum*. Toxins 6 (2). https://doi.org/10.3390/toxins6020575. Article 2.
Woo, S.L., Hermosa, R., Lorito, M., Monte, E., 2023. *Trichoderma*: a multipurpose, plant-beneficial microorganism for eco-sustainable agriculture. Nat. Rev. Microbiol. 21 (5), 312–326. https://doi.org/10.1038/s41579-022-00819-5.
Xu, X., Xi, N., Chen, J., Zhou, Z., Liu, M., Yan, G., Liu, Y., 2024. Deoxynivalenol exposure induces oxidative stress and apoptosis in human keratinocytes via PI3K/Akt and MAPK signaling pathway. Environ. Toxicol. 39 (1), 277–288. https://doi.org/10.1002/tox.23943.
Yaakoub, H., Mina, S., Calenda, A., Bouchara, J.-P., Papon, N., 2022. Oxidative stress response pathways in fungi. Cell. Mol. Life Sci. 79 (6), 333. https://doi.org/10.1007/s00018-022-04353-8.
Yoon, J.E., Lee, K.Y., Seok, J.S., Cheng, W.N., Kwon, H.C., Jeong, C.H., Han, S.G., 2019. Zearalenone induces endoplasmic reticulum stress and modulates the expression of phase I/II enzymes in human liver cells. Toxins 12 (1), 2. https://doi.org/10.3390/toxins12010002.